Quantitative basis for neuroimaging of cortical laminae with calibrated functional MRI

Peter Herman[a,b], Basavaraju G. Sanganahalli[a,b], Hal Blumenfeld[c,d], Douglas L. Rothman[a,b,e], and Fahmeed Hyder[a,b,e,1]

[a]Magnetic Resonance Research Center and Departments of [b]Diagnostic Radiology, [e]Biomedical Engineering, [c]Neurology, and [d]Neurobiology, Yale University, New Haven, CT 06520

Layer-specific neurophysiologic, hemodynamic, and metabolic measurements are needed to interpret high-resolution functional magnetic resonance imaging (fMRI) data in the cerebral cortex. We examined how neurovascular and neurometabolic couplings vary vertically in the rat's somatosensory cortex. During sensory stimulation we measured dynamic layer-specific responses of local field potential (LFP) and multiunit activity (MUA) as well as blood oxygenation level-dependent (BOLD) signal and cerebral blood volume (CBV) and blood flow (CBF), which in turn were used to calculate changes in oxidative metabolism (CMR_{O2}) with calibrated fMRI. Both BOLD signal and CBV decreased from superficial to deep laminae, but these responses were not well correlated with either layer-specific LFP or MUA. However, CBF changes were quite stable across laminae, similar to LFP. However, changes in CMR_{O2} and MUA varied across cortex in a correlated manner and both were reduced in superficial lamina. These results lay the framework for quantitative neuroimaging across cortical laminae with calibrated fMRI methods.

spike rate | electroencephalography | glutamate | neuroenergetics | lactate

The most recognizable features of the cerebral cortex across phyla are the layers (i.e., laminae) representing different cell types that project and connect to create networks, both in the horizontal and vertical directions of the cortex (1). Functional MRI (fMRI) with high-field magnets has been used to image this complex heterogeneous system of connections across cortical laminae. Given the complexity of the blood oxygenation level-dependent (BOLD) signal (2), quantitative assessment of neurophysiologic, hemodynamic, and metabolic responses across cortical laminae is needed to interpret high-resolution fMRI data in terms of neural activity. Because synaptic density (1) and commensurate electrical and chemical activities vary across cortical layers (3, 4), it is hypothesized that hemodynamic and metabolic responses would also vary. However, there are limited results on layer-specific variations in these parameters.

High magnetic fields have improved BOLD sensitivity and specificity (5), whereas other MRI developments have allowed cerebral blood volume (CBV) and flow (CBF) measurements to calibrate fMRI signal so that changes in cerebral metabolic rate of oxygen consumption (CMR_{O2}) can be calculated with a biophysical model of BOLD (6). These multimodal fMRI techniques in conjunction with other related magnetic resonance spectroscopy methods have allowed quantitative insights into the molecular and cellular bases of neurovascular and neurometabolic couplings (7).

In vivo recordings of neural activity with metal microelectrodes depict fluctuations of extracellular voltage, where the high- and low-frequency components, respectively, reflect multiunit activity (MUA) and local field potential (LFP) in a region (8). MUA is believed to reflect the output spiking activity of an ensemble of neurons because it reveals action potentials of large pyramidal neurons, whereas LFP reflects the synaptic input of a particular region because it depicts the weighted sum of changing membrane potentials along dendritic branches and soma (9, 10).

To interpret the functional organization of the mammalian cerebral cortex from high-resolution fMRI data, the relation of the BOLD signal to underlying neural activities and hemodynamic or metabolic responses is needed at the laminar level. Although many animal studies have contributed to our knowledge about fMRI and its relation to multimodal functional responses (9–16), these past reports have focused primarily on dynamic correlations of signals in a specific cortical region. Here we measured the degree to which neurovascular and neurometabolic couplings vary in the vertical direction of the rat's primary somatosensory cortex. Briefly, our results show that during sensory stimulation transcortical BOLD and CBV response patterns are uncoupled with both neural activity measures across cortical laminae, whereas neurometabolic coupling of MUA vs. CMR_{O2} and neurovascular coupling of LFP vs. CBF have different spatial distributions in the superficial lamina.

Results

During forepaw stimulation in the rat we measured dynamic responses of BOLD, CBV, and CBF at 11.7 T with different fMRI methods and then combined these data to calibrate the fMRI signal to calculate changes of CMR_{O2} (Eq. 1). Both BOLD and CBV were measured by gradient-echo contrast with 1-s temporal resolution. Spin-echo contrast, which has slightly different BOLD origins (17), was not used because of its lower contrast-to-noise ratio and because most prior neurophysiological bases of fMRI used the gradient-echo BOLD signal (9, 10). Although both gradient echo and spin echo have BOLD sensitivity, the difference between the transverse relaxation rates with gradient echo (R_2^*) and spin echo (R_2) shows that gradient echo has the largest BOLD component (i.e., $R_2' = R_2^* - R_2$) (18). CBV was measured with ferumoxtran, a plasma-borne intravascular paramagnetic contrast agent (19). CBF was recorded inside the magnet by arterial spin labeling (ASL) and on the bench by laser Doppler flowmetry (LDF). Because CBF measured by MRI had poorer temporal resolution (i.e., 10 s) compared with BOLD and/or CBV, we used the ASL data for spatial mapping of CBF and the LDF data for dynamic representation of CBF by scaling the laminar optical signals to the magnitude of the MRI-measured laminar responses (10, 19). The LDF probe was used in conjunction with high-impedance microelectrodes to record LFP and MUA simultaneously with CBF (10). The multimodal fMRI data had sufficient spatial resolution to separate the somatosensory cortex into several

Significance

This work challenges the notion that conventional functional magnetic resonance imaging (fMRI), that is, blood oxygenation level-dependent signal alone, can accurately reflect laminar neural activity. Instead, we show that calibrated fMRI methods for metabolic and hemodynamic measurements can better reflect laminar neuronal activities.

NEUROSCIENCE

nonoverlapping voxels located vertically along the forepaw area (i.e., upper, middle, and lower segments), whereas we used electrical/LDF data from three distinct but similarly sized segments, each with a thickness of ~0.6 mm (*Materials and Methods*).

Electrical and Multimodal fMRI Recordings Across Laminae. The averaged multimodal functional responses across different lamina from the contralateral somatosensory cortex during 30 s of forepaw stimulation are summarized in Fig. 1. For each modality, we first examine dynamic temporal patterns and then compare magnitudes across laminae.

The modality-specific response rise times and decay times of the fMRI data across cortical laminae are shown in Table S1 (one-way ANOVA). The rise-time constants for the multimodal fMRI signals (i.e., CBF < CBV < BOLD) were in good agreement with prior rat studies (20–26). In comparison with the fMRI data, the electrical data showed much faster transitions. For both MUA and LFP, the laminar neural changes were immediate following stimulation onset and offset (Fig. 1 *E* and *F*). However, immediately after stimulation onset an initial peak was observed that plateaued within a few seconds to roughly half of the initial peak at steady state. The neural data had quite typical time courses (9, 10, 16).

For BOLD, in relation to the response from the middle segment, the responses from upper and lower segments were 53% more and 33% less, respectively (Fig. 1*A*). The CBV responses were somewhat similar. In relation to the CBV response from the middle segment, the CBV responses from upper and lower segments were 11% more and 56% less, respectively (Fig. 1*B*). However, the CBF responses had a slight response attenuation from upper to lower segments, varying by at most 5–10% from upper to lower segments, where similar laminar flow distributions were observed with optical and MRI measurements (Fig. 1*C*). The spatial representation of CMR_{O_2} was quite different from the patterns of BOLD, CBV, and CBF data (Fig. 1*D*). In relation to the CMR_{O_2} response from the middle segment, the CMR_{O_2} responses from upper and lower segments were 31% less and 10% more, respectively. The calculation of CMR_{O_2} changes was based on laminar patterns of BOLD, CBV, and CBF responses as well as the baseline BOLD signal as signified by the parameter M in Eq. **1** and assumptions about whether the CBV changes occurred in the venous vs. arterial compartment (27). The baseline BOLD signal, as measured by R_2' (*Materials and Methods*), in well-shimmed rat brain was measured to be quite homogenous in the somatosensory cortex (Fig. S1*A*). Current assumptions about BOLD signal are that the oxygenation and volume changes primarily occur at the venous end (2, 6, 27). However, the trend of the laminar CMR_{O_2} changes is minimally affected whether the CBV changes occurred in the venous or arterial compartment (Fig. S1*B*) or when M was allowed to vary by ±25% from the measured value (Fig. S1*C*). The neural responses as reflected by MUA and LFP were, respectively, similar to CMR_{O_2} and CBF. The MUA responses from the middle and lower segments were within 2% of each other, whereas the MUA response from the upper segment was 35% less (Fig. 1*E*). Similar to CBF, the LFP responses from all cortical segments were quite analogous (Fig. 1*F*), but with a slight peak in the middle segment. Although the spatial distributions of the multimodal fMRI responses are generally in reasonable agreement with past findings in the rat (20–26), particulars of these functional responses are examined further below (*Discussion*).

Laminar Functional Responses. The laminar neurovascular and neurometabolic couplings from functional responses are summarized in Fig. 2, Table S2, and Fig. S2. In the absolute scale the smallest and largest response magnitudes were observed with BOLD/CBV and CBF, respectively, whereas CMR_{O_2}, LFP, and MUA all had approximately similar scales (Fig. 1). The laminar variations became more apparent when the functional responses were normalized with respect to the response from the middle segment (Fig. 2).
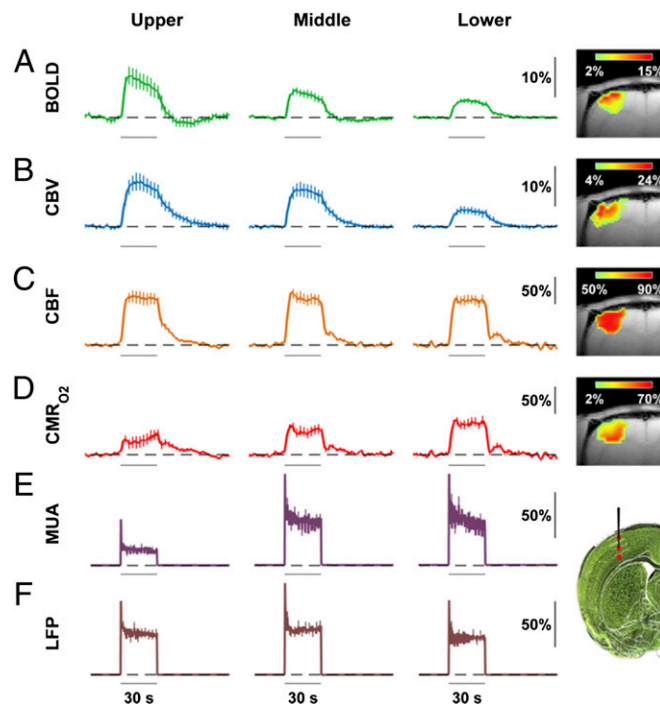

Fig. 1. Multimodal functional responses across cortical laminae (upper, middle, and lower segments, each ~600 μm thick; mean ± SEM). Averaged time courses are presented with 1-s time resolution and the SEMs are shown every 3 s for better visibility. The vertical axes are expressed as the relative change compared with the baseline (dashed line). Images on the right depict the spatial representation of typical single-trial activation maps ($P < 0.01$) as well as the sites of MUA and LFP recordings on a Nissl-stained image. (*A*) BOLD responses ($n = 12$) showed poststimulation dips of ~2% and ~1%, respectively, in upper and middle segments (Table S1). BOLD responses decreased from upper to middle to lower segments. (*B*) CBV responses ($n = 12$), similar to BOLD but measured with a plasma-borne contrast agent, showed slower signal decays compared with BOLD (Table S1). CBV responses reduced from upper/middle to lower segments also. (*C*) CBF responses ($n = 32$), measured respectively with ASL and LDF for spatial and dynamic representations, showed faster initial signal decays compared with BOLD and CBV (Table S1). CBF responses were generally uniform across layers, but with a tendency to decrease from upper to middle to lower segments. (*D*) CMR_{O_2} responses, calculated by calibrated fMRI (Eq. **1** and Fig. S1), showed variable spatial and dynamic patterns compared with BOLD, CBV, and CBF data (Table S1). CMR_{O_2} responses were smallest in the upper segment but similar in middle and lower segments. The SEM of CMR_{O_2} was calculated by Monte-Carlo simulation. (*E*) MUA responses ($n = 32$), measured by high-impedance microelectrodes, showed an initial peak immediately after stimulation onset and plateaued within 2–3 s. MUA responses were smallest in the upper segment but similar in middle and lower segments. (*F*) LFP responses ($n = 32$) measured simultaneously with the MUA showed an initial peak similar to the MUA data, but the LFP responses were somewhat uniform across layers, but with a slight peak in the middle segment. Fig. 2 gives details on statistical significance.

Both BOLD and CBV responses decreased from superficial to deep lamina. The BOLD laminar responses decreased by about 33% from upper to middle to lower segments, whereas the CBV laminar response decreased by more than 50% from upper/middle to lower segments. Neither of the neural responses from different layers behaved like the laminar responses for BOLD and CBV. The MUA laminar response in the upper layer response was less than 50% of responses from middle/lower segments. However, the LFP response in the middle segment peaked slightly above the other layers. The CBF and LFP patterns were analogous to each other, whereas the CMR_{O_2} and MUA patterns were quite comparable as well. Thus, spatial coupling was observed between CMR_{O_2} vs. CBF and MUA vs. LFP for the majority of the cerebral cortex (i.e., middle and lower segments).
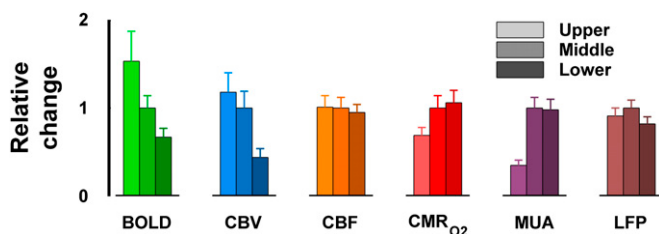
Fig. 2. Summary of multimodal functional responses. All data shown as means ± SEM (Fig. 1). Relative functional responses obtained by normalized values with respect to the response from the middle layer for each modality. Transition from upper to middle to lower segments are shown by darker shades (for each respective color/modality). Statistical analysis for BOLD data showed that all layer-specific comparisons were significant (i.e., upper vs. middle $P = 0.09$, upper vs. lower $P < 0.01$, and middle vs. lower $P < 0.05$), whereas for CBV data only upper vs. middle was insignificant (i.e., upper vs. lower $P < 0.002$ and middle vs. lower $P < 0.006$). BOLD responses decreased from upper to middle by ~50% and then by another ~50% from middle to lower segments, whereas CBV responses reduced from upper/middle to lower segments by ~60%. All layer-specific comparisons for CBF data were insignificant, but CBF responses decreased from upper/middle to lower segments by ~10%. Statistical analysis for CMR_{O2} data showed that only middle vs. lower was insignificant (i.e., upper vs. middle $P < 0.08$ and upper vs. lower $P < 0.006$), quite similar to the MUA data (i.e., upper vs. middle $P < 0.01$ and upper vs. lower $P < 0.001$). From middle/lower to upper segments CMR_{O2} responses reduced by ~30% and MUA responses decreased by ~50%. Like the CBF statistical analysis, the LFP data showed that all layer-specific comparisons were insignificant, but LFP responses peaked in the middle segment by ~20%. Table S2 and Fig. S2 give details on correlations.

The only discrepancy between MUA vs. LFP and CMR_{O2} vs. CBF was in the upper segment.

These similarities/differences of laminar responses for the different modalities were inspected further by a linear regression analysis by plotting the respective data points of response time course from one layer vs. another layer (Fig. S2). The slope of the regressions from all three permutations of segment comparisons (i.e., upper vs. middle, upper vs. lower, middle vs. lower) is shown in Table S2, where a slope of close to 1 (i.e., line of identity) suggested agreement between the two layer-specific responses. Both LFP and CBF showed good correspondence of responses across all layers. However, MUA and CMR_{O2} displayed respectable similarity of responses between middle and lower segments. The BOLD responses showed no resemblance of responses across layers and thus were completely uncoupled from either neural response. Although the CBV responses behaved generally similar to the BOLD responses, because of minimal difference between CBV responses in the upper and middle segments (Fig. 1B) the CBV exhibited similar responses between the upper vs. middle layers.

Laminar Transfer Functions. Transfer functions (h_X) establish a mathematical connection between input and output signals of a given system. In physiological modeling the transfer function between neural signals and the resulting hemodynamic or metabolic changes mathematically characterizes the neurovascular or neurometabolic couplings. We compared laminar transfer functions to emphasize the temporal relations of metabolic/hemodynamic signals with the underlying neural activity. We applied a convolution analysis to calculate layer-specific transfer functions for BOLD, CBV, and CBF with either neural response as the input (*SI Materials and Methods*). The CMR_{O2} transfer functions were based on the BOLD, CBV, and CBF transfer functions (i.e., with Eq. 1). The laminar neurovascular and neurometabolic couplings from transfer functions are shown in Table S3 and Figs. S3 and S4.

With laminar MUA as the input (Fig. S3A, *Top*), the layer-specific transfer functions for BOLD and CBV showed that the impulse peaks decrease significantly from upper to middle to lower segments, where the greatest drop-off was between upper

and middle segments. However, laminar transfer functions for CBF and CMR_{O2} showed negligible differences of the impulse peaks in middle and lower segments, whereas the impulse peaks of the upper segment were much larger than the impulse peaks of the other segments. In comparison, all transfer functions with laminar LFP as the input had much smaller impulse peaks (Fig. S3A, *Bottom*). The laminar transfer functions with layer-specific LFP seemed quite similar to the laminar transfer functions with layer-specific MUA. The basic features of the transfer functions for the multimodal responses are in good agreement with prior studies spanning various species (9, 10, 16).

We also conducted a correlation of the transfer functions (Fig. S3B). For a given modality, a linear regression analysis was performed by plotting the transfer function, with either neural response as the input, of one layer vs. another layer. The slope of the regressions from all three permutations of segment comparisons (i.e., upper vs. middle, upper vs. lower, and middle vs. lower) is shown in Table S3, where a slope of close to 1 (i.e., line of identity) indicated correspondence between the two layer-specific transfer functions. Whereas the regression values for correlation between layer-specific transfer functions for every modality are summarized in Table S3 and Fig. S3B, the main highlights of laminar neurovascular (i.e., LFP vs. CBF) and neurometabolic (i.e., MUA vs. CMR_{O2}) couplings from transfer functions are shown in Fig. S4.

Generally, the result of the regression analysis with layer-specific transfer functions (Table S3) and outcome of the regression analysis with layer-specific functional responses (Table S2) were quite similar. CMR_{O2} transfer functions derived from MUA (h_{CMRO2}; Fig. S4A, *Top*) for the middle and lower segments were interchangeable (Fig. S4B, *Top*), whereas the CBF transfer functions derived from LFP (h_{CBF}; Fig. S4A, *Bottom*) for all layers were quite similar and therefore easily swapped (Fig. S4B, *Bottom*). For each modality, the mean of the laminar regression values from all three permutations of segment comparisons (i.e., upper vs. middle, upper vs. lower, and middle vs. lower) provided an estimate of the overall predictive power of the respective transfer function (i.e., a value close to 1 indicates higher predictive power). Comparing the mean of the layer-specific regression values for all modalities illustrates that h_{CMRO2} and h_{CBF}, compared with all other transfer functions, had maximum accuracy to predict MUA and LFP, respectively (Fig. S4C).

Modeling Neural Responses with Wiener Deconvolution. We tested the proposition that h_{CMRO2} and h_{CBF} had high predictability for neural responses (Fig. S4). We used the Wiener deconvolution approach to calculate the neural responses (*SI Materials and Methods*). New datasets were not needed in prediction of neural signals. We used the transfer functions of BOLD, CBV, CBF, and CMR_{O2} (i.e., h_{BOLD}, h_{CBV}, h_{CBF}, and h_{CMRO2} as in Fig. S3A, but only their respective averages) in conjunction with the measured laminar BOLD, CBV, CBF, and CMR_{O2} responses (i.e., as in Fig. 1 A–D for all segments) to predict the laminar neural responses, which were then compared with the measured laminar neural responses (i.e., as in Fig. 1 E and F for all segments). A residual analysis was used to estimate the accuracy of the prediction. For a given modality x, a residual value (R_x) was calculated using the root mean square of the difference between predicted and measured responses for the entire duration of the dataset. Because a smaller R_x value indicated better fit to the data, we used the sum of R_x values across all cortical layers (ΣR_x) to reflect the predictive power of the neural responses (Table S4).

Although the ability to calculate neural responses for middle and lower segments from the averaged transfer functions of BOLD, CBV, CBF, and CMR_{O2} were all quite good, the predictive power for neural responses in the upper segment from the averaged transfer functions of CBF and CMR_{O2} were far superior (Table S4). In other words, the BOLD and CBV responses were highly uncoupled from neural responses predominantly in the superficial layer, whereas the overall ability to predict laminar MUA and LFP, respectively, from the averaged transfer functions for CMR_{O2} and CBF were far superior (Fig. 3). Because

NEUROSCIENCE

comparison between measured and predicted responses of MUA and LFP across cortical laminae showed small differences when the averaged transfer functions of CMR_{O2} (Fig. 3A) and CBF (Fig. 3B) were used, we conclude that these neural activities have the strongest correlations with metabolic and hemodynamic responses, respectively. In other words, the CMR_{O2} and CBF transfer functions representing the entire cortical depth may be experimentally sufficient to represent MUA and LFP, respectively, across cortical laminae. This may have consequences for being able to reliably use CMR_{O2} and CBF for quantitative neuroimaging in humans where spatial resolution may not be sufficient to separate the cortical segments in all parts of the cerebrum (Discussion).

Discussion

Although the spatial resolution in this study was not at the level of "anatomical" cortical layers, we were able to split the cortex into three operationally distinct segments—each about 600 µm along the vertical dimension denoted upper, middle, and lower, respectively—which corresponded roughly to layers I–III, IV–V, and VI in the rat (28). Briefly, the upper segment consists of neurons projecting to other adjacent cortical areas, the middle segment contains inputs from the thalamus and projections to the spinal cord, and the lower segment has reciprocal connections to and from deeper regions (1). About 80% of cortical neurons are excitatory, which use glutamate as the neurotransmitter and of which larger pyramidal neurons dominate, whereas the remaining fraction is primarily the smaller inhibitory neurons that mostly use GABA as the neurotransmitter (29). Although the total neuronal density is slightly higher in the middle segment, the fraction of GABA neurons in the upper segment is double that in middle and lower segments (28). Densities of cerebral capillaries and cytochrome oxidase are well correlated with blood flow and glucose metabolism at rest (30–32), all of which seem to peak in the middle/lower segments.

Laminar Responses of Imaging and Neural Signals. Neither BOLD nor CBV response patterns were coupled to either measure of neural response. However, there was strong spatial association between LFP and CBF response patterns, but this coupling was slightly different from the correspondence between MUA and CMR_{O2}, specifically in superficial lamina. Thus, high-resolution BOLD or CBV imaging cannot properly reflect laminar neural activity. If, however, BOLD and CBV imaging is combined with CBF mapping—as in calibrated fMRI for CMR_{O2}—independent

use of metabolic and hemodynamic signals may provide better surrogates for laminar neuroimaging of MUA and LFP, respectively.

There are two important consequences of the findings that both LFP and CBF were uniform across cortical lamina, whereas both MUA and CMR_{O2} were smaller, mainly in the superficial lamina. First, the averaged laminar transfer functions of CMR_{O2} (derived from MUA) and CBF (derived from LFP) may predict laminar neural responses in situations where MRI spatial resolution is insufficient to separate cortical lamina. Second, neurovascular (i.e., LFP vs. CBF) and neurometabolic (i.e., MUA vs. CMR_{O2}) couplings exist mainly in deeper laminae, thereby suggesting that LFP and MUA as well as CBF and CMR_{O2} are potentially uncoupled superficially.

Comparison with Previous Cortical Laminar Measurements. The patterns of multimodal fMRI results across cortical laminae—past experiments that were conducted at magnetic fields ranging from 4.7T to 11.7 T—are in reasonable agreement with our results (20–26, 33, 34). The spatial distributions of MUA and LFP responses across cortical laminae are mostly in congruence with layer-specific neural measurements across various animal models (34–40).

Regardless of the anesthetic, rat studies consistently show that the upper segment produced the strongest BOLD response, whereas the lower segment generated the weakest response (20–26, 33, 34). Similar to the BOLD data, the drop-off in magnitude for the CBV response in the rat was greatest in the lower segment (20, 24–26, 34). For example, similar to our CBV results at 11.7 T with α-chloralose anesthesia, Hirano et al. (26) found CBV responses to be significantly lower in deeper lamina using experimental conditions similar to ours, whereas Shen et al. (25) at 4.7 T with isoflurane anesthesia found CBV response to peak in the upper/middle segments. Recent BOLD and CBV results in primate brain agree well with the rat results (41). Because the larger pial vessels are located mostly in the superficial lamina, BOLD and CBV responses are much greater (30, 31) in these regions.

Past laminar CBF responses are generally agreeable with our findings (20–23, 25, 26, 33, 41). In rat brain, Shen et al. (25) observed that the CBF response is about 30% smaller in the upper segment (vs. other layers) with 20 s of forepaw stimulation, whereas Hirano et al.(26) found that the CBF response is about 50% smaller in the lower segment (vs. other layers) using very short (<2 s) forepaw stimuli. In primate brain, Goense et al. (41) found CBF response to be variable with stimulus conditions, ranging from attenuation from upper to middle to lower segments (i.e., similar to BOLD/CBV) to 40% peaking in the middle segment (vs. other layers). Differences across these studies could be due to partial volume variations, anesthetic effects on blood flow, species-specific effects, stimulus duration dissimilarity leading to variable adaptation, and/or type of ASL sequence used. In our rat study, where we used 30 s of forepaw stimulation with α-chloralose anesthesia, we found that the magnitudes of laminar CBF responses decreased by 5–10% from upper to lower segments. Because ASL requires homogenous magnetic labeling for CBF contrast (33, 42), there is potential for experimental variations due to distribution and/or efficiency of the labeling from subject to subject. Thus, improved CBF methods are needed because CBF has slightly lower sensitivity compared with BOLD and CBV (6).

Few studies have investigated the laminar CMR_{O2} patterns with calibrated fMRI, which require BOLD, CBV, and CBF measurements in the same subject. Rat autoradiographic studies, which measure changes in glucose consumption during protracted sensory stimulation, have shown either uniform metabolism across most layers (43) or slightly higher metabolism in the middle/lower segments (vs. upper segment) (44). Of all of the multimodal fMRI studies reviewed above in the context of laminar responses, only Shen et al. (25) calculated CMR_{O2} to find the laminar variations to mimic exactly the layer-specific metabolic changes we report here. Furthermore given the laminar distributions of BOLD, CBV, and CBF in the Hirano et al. (26) study, which had very different stimulus durations than in our study, we
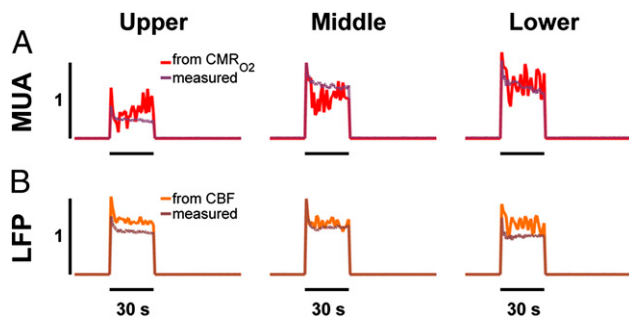

Fig. 3. Predictive power of neural activity from averaged transfer functions for CMR_{O2} (h_{CMRO2}) and CBF (h_{CBF}) derived, respectively, from MUA and LFP as the inputs. Neural response was predicted by the Wiener deconvolution algorithm (SI Materials and Methods) using the average of transfer functions obtained across layers for a given modality. (A) Comparison of measured and predicted MUA responses from cortical lamina by using the average h_{CMRO2}. (B) Comparison of measured and predicted LFP responses from cortical lamina by using the average h_{CBF}. The predictive power of neural responses was based on a residual analysis (SI Materials and Methods), which was based on the difference between predicted and measured neural responses. Fig. S4 and Table S4 give details on predictive powers of all other transfer functions.

expect that the laminar CMR_{O2} variations could mirror the metabolic trends in our study. The lower CMR_{O2} in superficial lamina could basically reflect the reduced energy demand of smaller number of pyramidal neurons (4) whereas the high CBF in the upper layer could reflect the perfusion in penetrating arterioles (26).

The spatial patterns of MUA and LFP responses across cortical laminae are difficult to compare because few studies tend to measure these signals together during sensory stimulation (9, 10). Regardless of anesthetics used and across species (34–40), the absolute magnitude of the LFP is shown to be quite equivalent across layers (34–36), whereas the MUA seems to peak from the middle to the lower segments (34, 37, 38). Laminar multielectrode measurements of LFP and MUA in the somatosensory areas after stimulation showed a pattern similar to that observed in our study (34, 45). In addition, the overall MUA laminar trend in this study seems to correspond with a recent meta-analysis of sensory-evoked changes in spiking activity in various rat models (4).

Spatial Uncoupling in the Superficial Layers. Not many calibrated fMRI studies have investigated the spatial uncoupling between CMR_{O2} and CBF along the vertical direction of the cortex (25, 26). However, Malonek and Grinvald (46), using an optical and electrical combined study, were the first to point to the possibility of a spatial mismatch between CMR_{O2} and CBF at a certain cortical depth. In the cat they combined recordings of intrinsic signals (i.e., oxyhemoglobin and deoxyhemoglobin) with MUA during visual stimulation. The electrical data were recorded from layer IV, whereas the optical data represented an integrated average of responses from upper to middle segments. They found that the map of the evoked neural response agreed much better with the functional map of the deoxyhemoglobin signal (i.e., reflecting CMR_{O2} increase) than the functional map of the oxyhemoglobin signal (i.e., reflecting CBF increase). Given the much better spatial overlap between the neural and metabolic maps compared with the neural and flow maps, Malonek and Grinvald (46) coined the phrase "watering the entire garden for the sake of one thirsty flower." In agreement with this observation, autoradiographic studies of rat somatosensory activation show that blood flow response is distributed over a larger area than the glucose metabolic response, especially in the superficial layers (47). This concept of flow–metabolism spatial uncoupling is the foundation for columnar mapping with optical imaging and fMRI (i.e., differential mapping of oxyhemoglobin and deoxyhemoglobin signals) under various behavioral conditions and across species (48–50). However, future studies are needed to extend these types of measurements for quantitative neuroimaging.

Recent electrophysiological studies (51–53) suggest the potential for spatial uncoupling between LFP and MUA. Using electrode arrays oriented in either vertical or horizontal directions of the cerebral cortex, the results suggest that LFP spreads much farther than the MUA because of "volume-conducted" field potentials across far distances (52), thus making LFP reflective of global activity in addition to the more localized MUA-based signal. Thus, the MUA reflects electrical activity within small domains of several hundred micrometers at most, whereas the LFP seems to mimic the MUA but in addition also captures activity across larger distances. These experimental findings are in agreement with recent biophysical studies that suggest that correlation of synaptic activity (54) and/or microscale inhomogeneity arising from different cell populations could be dominant factors for electric field propagation (55). Thus, the point-spread functions of fMRI and LFP are comparable, but not for MUA (i.e., BOLD ≈ LFP > MUA; *Materials and Methods*).

A potential consequence is that the "global" measure of LFP signal would give better temporal correlation to the BOLD response than the "local" MUA. These recent observations may explain the finding by Logothetis et al. (9), who had previously reported in the primate visual cortex that the correlation is slightly better for BOLD vs. LFP (r^2 mean of 0.52) than BOLD vs. MUA (r^2 mean of 0.45). Because high-impedance microelectrodes, as used in these types of studies, including ours, are biased toward voltage fluctuations of the larger pyramidal neurons, it is possible that the MUA signal is unable to accurately reflect the activity of the smaller nonpyramidal neurons. Because the GABAergic neuronal population is much higher in the upper segment (28), it is likely that the laminar MUA responses may be more reflective of the variable glutamatergic neuronal population across cortical laminae [i.e., being higher in middle and lower segments (28)]. If so, then LFP is more characteristic of neural activity of both glutamatergic and GABAergic neurons across cortical laminae. However, clearly more studies are needed to confirm these suggestions.

In summary, the present results challenge the notion that "conventional fMRI"—i.e., BOLD alone—can accurately reflect laminar neural activity. Instead, the results suggest that "calibrated fMRI," which is available for translational use for metabolic and hemodynamic imaging (6, 56), may be better suited for quantitative laminar neuroimaging of spiking activity and field potential respectively.

Materials and Methods

All procedures were performed in accordance with approved protocols as previously described (10, 19, 57, 58). Briefly, rats were anesthetized with α-chloralose and prepared for fMRI and electrophysiology studies (57). All physiological parameters were maintained within normal limits for the entire duration of the study. Multimodal fMRI studies with electrical forepaw stimulation were conducted at 11.7 T with echo-planar imaging (EPI) using previously used contrasts for BOLD, CBV, and CBF measured in fractional changes from the resting baseline condition (18, 33, 59). The in-plane point-spread function of an EPI voxel was 450×450 μm (with 2-mm slice thickness). Changes in CMR_{O2} were calculated by calibrated fMRI:

$$\frac{\Delta CMR_{O2}}{CMR_{O2}} = \frac{\Delta CBF}{CBF} - \left(\frac{1}{M}\frac{\Delta S}{S} + \frac{\Delta CBV}{CBV}\right)\left(1 + \frac{\Delta CBF}{CBF}\right), \quad [1]$$

where S is the BOLD signal and the value of M is given by the product between echo time (TE) and R_2', which is given by the absolute difference between the transverse relaxation rates with gradient echo (R_2^*) and spin echo (R_2) (i.e., $R_2' = R_2^* - R_2$). Under well-shimmed conditions, the R_2^* and R_2 maps were measured with several TE values. Fig. S1A shows a typical R_2' map, where about ±5% variation is observed across lamina. The mean cortical R_2' value of 26.5 ± 3 s^{-1} gives an equivalent M value of 0.4 ± 0.04 with a TE of 15 ms. Nevertheless, CMR_{O2} changes were calculated with M ranging from 0.3 to 0.5 (10, 60). Electrophysiological recordings from three depths of the forepaw region were made with high-impedance microelectrodes, which were combined with a LDF probe for simultaneous CBF measurements (10, 19). Because the interoptode distance for the LDF probe was 200 μm, the effective spatial resolution of LDF was a half-ellipsoid ~0.1-μL volume. The sensitive volumes for LFP and MUA were estimated as spheres with diameters of about 600 and 200 μm, respectively (61). MUA and LFP were extracted from the raw extracellular signal using high band-pass (300–3,000 Hz) and low-pass (<150 Hz) electronic filters (10). All other experimental details and description of data analysis (e.g., transfer function, correlations, etc.) are described in *SI Materials and Methods*.

1. Shepherd GM (2004) *The Synaptic Organization of the Brain* (Oxford Univ Press, New York).
2. Ogawa S, et al. (1993) Functional brain mapping by blood oxygenation level-dependent contrast magnetic resonance imaging. A comparison of signal characteristics with a biophysical model. *Biophys J* 64(3):803–812.
3. Riera JJ, Schousboe A, Waagepetersen HS, Howarth C, Hyder F (2008) The micro-architecture of the cerebral cortex: Functional neuroimaging models and metabolism. *Neuroimage* 40(4):1436–1459.

4. Hyder F, Rothman DL, Bennett MR (2013) Cortical energy demands of signaling and nonsignaling components in brain are conserved across mammalian species and activity levels. *Proc Natl Acad Sci USA* 110(9):3549–3554.
5. Uğurbil K (2012) The road to functional imaging and ultrahigh fields. *Neuroimage* 62(2):726–735.
6. Pike GB (2012) Quantitative functional MRI: Concepts, issues and future challenges. *Neuroimage* 62(2):1234–1240.

7. Hyder F, Rothman DL (2012) Quantitative fMRI and oxidative neuroenergetics. *Neuroimage* 62(2):985–994.
8. Buzsaki G (2006) *Rhythms of the Brain* (Oxford Univ Press, New York).
9. Logothetis NK, Pauls J, Augath M, Trinath T, Oeltermann A (2001) Neurophysiological investigation of the basis of the fMRI signal. *Nature* 412(6843):150–157.
10. Sanganahalli BG, Herman P, Blumenfeld H, Hyder F (2009) Oxidative neuroenergetics in event-related paradigms. *J Neurosci* 29(6):1707–1718.
11. Ances BM, Buerk DG, Greenberg JH, Detre JA (2001) Temporal dynamics of the partial pressure of brain tissue oxygen during functional forepaw stimulation in rats. *Neurosci Lett* 306(1-2):106–110.
12. Smith AJ, et al. (2002) Cerebral energetics and spiking frequency: the neurophysiological basis of fMRI. *Proc Natl Acad Sci USA* 99(16):10765–10770.
13. Heeger DJ, Ress D (2002) What does fMRI tell us about neuronal activity? *Nat Rev Neurosci* 3(2):142–151.
14. Thompson JK, Peterson MR, Freeman RD (2005) Separate spatial scales determine neural activity-dependent changes in tissue oxygen within central visual pathways. *J Neurosci* 25(39):9046–9058.
15. Mukamel R, et al. (2005) Coupling between neuronal firing, field potentials, and FMRI in human auditory cortex. *Science* 309(5736):951–954.
16. Martin C, Martindale J, Berwick J, Mayhew J (2006) Investigating neural-hemodynamic coupling and the hemodynamic response function in the awake rat. *Neuroimage* 32(1):33–48.
17. Zhao F, Wang P, Hendrich K, Ugurbil K, Kim SG (2006) Cortical layer-dependent BOLD and CBV responses measured by spin-echo and gradient-echo fMRI: Insights into hemodynamic regulation. *Neuroimage* 30(4):1149–1160.
18. Kida I, Kennan RP, Rothman DL, Behar KL, Hyder F (2000) High-resolution CMR(O2) mapping in rat cortex: A multiparametric approach to calibration of BOLD image contrast at 7 Tesla. *J Cereb Blood Flow Metab* 20(5):847–860.
19. Herman P, Sanganahalli BG, Hyder F (2009) Multimodal measurements of blood plasma and red blood cell volumes during functional brain activation. *J Cereb Blood Flow Metab* 29(1):19–24.
20. Kida I, Rothman DL, Hyder F (2007) Dynamics of changes in blood flow, volume, and oxygenation: Implications for dynamic functional magnetic resonance imaging calibration. *J Cereb Blood Flow Metab* 27(4):690–696.
21. Silva AC, Lee SP, Yang G, Iadecola C, Kim SG (1999) Simultaneous blood oxygenation level-dependent and cerebral blood flow functional magnetic resonance imaging during forepaw stimulation in the rat. *J Cereb Blood Flow Metab* 19(8):871–879.
22. Silva AC, Koretsky AP (2002) Laminar specificity of functional MRI onset times during somatosensory stimulation in rat. *Proc Natl Acad Sci USA* 99(23):15182–15187.
23. Duong TQ, Silva AC, Lee SP, Kim SG (2000) Functional MRI of calcium-dependent synaptic activity: Cross correlation with CBF and BOLD measurements. *Magn Reson Med* 43(3):383–392.
24. Keilholz SD, Silva AC, Raman M, Merkle H, Koretsky AP (2006) BOLD and CBV-weighted functional magnetic resonance imaging of the rat somatosensory system. *Magn Reson Med* 55(2):316–324.
25. Shen Q, Ren H, Duong TQ (2008) CBF, BOLD, CBV, and CMRO(2) fMRI signal temporal dynamics at 500-msec resolution. *J Magn Reson Imaging* 27(3):599–606.
26. Hirano Y, Stefanovic B, Silva AC (2011) Spatiotemporal evolution of the functional magnetic resonance imaging response to ultrashort stimuli. *J Neurosci* 31(4):1440–1447.
27. Hyder F, et al. (2010) Neurovascular and neurometabolic couplings in dynamic calibrated fMRI: Transient oxidative neuroenergetics for block-design and event-related paradigms. *Front Neuroenergetics* 2(18): 10.3389/fnene.2010.00018.
28. Beaulieu C (1993) Numerical data on neocortical neurons in adult rat, with special reference to the GABA population. *Brain Res* 609(1-2):284–292.
29. Winfield DA, Gatter KC, Powell TP (1980) An electron microscopic study of the types and proportions of neurons in the cortex of the motor and visual areas of the cat and rat. *Brain* 103(2):245–258.
30. Klein B, Kuschinsky W, Schröck H, Vetterlein F (1986) Interdependency of local capillary density, blood flow, and metabolism in rat brains. *Am J Physiol* 251(6 Pt 2):H1333–H1340.
31. Borowsky IW, Collins RC (1989) Metabolic anatomy of brain: A comparison of regional capillary density, glucose metabolism, and enzyme activities. *J Comp Neurol* 288(3):401–413.
32. Wong-Riley MT (1989) Cytochrome oxidase: An endogenous metabolic marker for neuronal activity. *Trends Neurosci* 12(3):94–101.
33. Kida I, Maciejewski PK, Hyder F (2004) Dynamic imaging of perfusion and oxygenation by functional magnetic resonance imaging. *J Cereb Blood Flow Metab* 24(12):1369–1381.
34. Shih YY, et al. (2013) Ultra high-resolution fMRI and electrophysiology of the rat primary somatosensory cortex. *Neuroimage* 73:113–120.
35. Devor A, et al. (2003) Coupling of total hemoglobin concentration, oxygenation, and neural activity in rat somatosensory cortex. *Neuron* 39(2):353–359.
36. Hewson-Stoate N, Jones M, Martindale J, Berwick J, Mayhew J (2005) Further non-linearities in neurovascular coupling in rodent barrel cortex. *Neuroimage* 24(2):565–574.
37. Derdikman D, et al. (2006) Layer-specific touch-dependent facilitation and depression in the somatosensory cortex during active whisking. *J Neurosci* 26(37):9538–9547.
38. Xing D, Yeh CI, Shapley RM (2009) Spatial spread of the local field potential and its laminar variation in visual cortex. *J Neurosci* 29(37):11540–11549.
39. Burns SP, Xing D, Shapley RM (2010) Comparisons of the dynamics of local field potential and multiunit activity signals in macaque visual cortex. *J Neurosci* 30(41):13739–13749.
40. Nemoto M, et al. (2012) Diversity of neural-hemodynamic relationships associated with differences in cortical processing during bilateral somatosensory activation in rats. *Neuroimage* 59(4):3325–3338.
41. Goense J, Merkle H, Logothetis NK (2012) High-resolution fMRI reveals laminar differences in neurovascular coupling between positive and negative BOLD responses. *Neuron* 76(3):629–639.
42. Silva AC, Kim SG (1999) Pseudo-continuous arterial spin labeling technique for measuring CBF dynamics with high temporal resolution. *Magn Reson Med* 42(3):425–429.
43. Ueki M, Linn F, Hossmann KA (1988) Functional activation of cerebral blood flow and metabolism before and after global ischemia of rat brain. *J Cereb Blood Flow Metab* 8(4):486–494.
44. Kossut M, Hand PJ, Greenberg J, Hand CL (1988) Single vibrissal cortical column in SI cortex of rat and its alterations in neonatal and adult vibrissa-deafferented animals: a quantitative 2DG study. *J Neurophysiol* 60(2):829–852.
45. Einevoll GT, et al. (2007) Laminar population analysis: estimating firing rates and evoked synaptic activity from multielectrode recordings in rat barrel cortex. *J Neurophysiol* 97(3):2174–2190.
46. Malonek D, Grinvald A (1996) Interactions between electrical activity and cortical microcirculation revealed by imaging spectroscopy: Implications for functional brain mapping. *Science* 272(5261):551–554.
47. Greenberg JH, Sohn NW, Hand PJ (1999) Nitric oxide and the cerebral-blood-flow response to somatosensory activation following deafferentation. *Exp Brain Res* 129(4):541–550.
48. Shtoyerman E, Arieli A, Slovin H, Vanzetta I, Grinvald A (2000) Long-term optical imaging and spectroscopy reveal mechanisms underlying the intrinsic signal and stability of cortical maps in V1 of behaving monkeys. *J Neurosci* 20(21):8111–8121.
49. Fukuda M, Moon CH, Wang P, Kim SG (2006) Mapping iso-orientation columns by contrast agent-enhanced functional magnetic resonance imaging: Reproducibility, specificity, and evaluation by optical imaging of intrinsic signal. *J Neurosci* 26(46):11821–11832.
50. Yacoub E, Harel N, Ugurbil K (2008) High-field fMRI unveils orientation columns in humans. *Proc Natl Acad Sci USA* 105(30):10607–10612.
51. Gawne TJ (2010) The local and non-local components of the local field potential in awake primate visual cortex. *J Comput Neurosci* 29(3):615–623.
52. Kajikawa Y, Schroeder CE (2011) How local is the local field potential? *Neuron* 72(5):847–858.
53. Gaucher Q, Edeline JM, Gourévitch B (2012) How different are the local field potentials and spiking activities? Insights from multi-electrodes arrays. *J Physiol Paris* 106(3-4):93–103.
54. Lindén H, et al. (2011) Modeling the spatial reach of the LFP. *Neuron* 72(5):859–872.
55. Nelson MJ, Bosch C, Venance L, Pouget P (2013) Microscale inhomogeneity of brain tissue distorts electrical signal propagation. *J Neurosci* 33(7):2821–2827.
56. Qiu D, Zaharchuk G, Christen T, Ni WW, Moseley ME (2012) Contrast-enhanced functional blood volume imaging (CE-fBVI): Enhanced sensitivity for brain activation in humans using the ultrasmall superparamagnetic iron oxide agent ferumoxytol. *Neuroimage* 62(3):1726–1731.
57. Sanganahalli BG, Bailey CJ, Herman P, Hyder F (2009) Tactile and non-tactile sensory paradigms for fMRI and neurophysiologic studies in rodents. *Methods Mol Biol* 489:213–242.
58. Herman P, Sanganahalli BG, Hyder F, Eke A (2011) Fractal analysis of spontaneous fluctuations of the BOLD signal in rat brain. *Neuroimage* 58(4):1060–1069.
59. Lu H, Scholl CA, Zuo Y, Stein EA, Yang Y (2007) Quantifying the blood oxygenation level dependent effect in cerebral blood volume-weighted functional MRI at 9.4T. *Magn Reson Med* 58(3):616–621.
60. Hyder F, et al. (2001) Quantitative functional imaging of the brain: Towards mapping neuronal activity by BOLD fMRI. *NMR Biomed* 14(7-8):413–431.
61. Bédard C, Kröger H, Destexhe A (2004) Modeling extracellular field potentials and the frequency-filtering properties of extracellular space. *Biophys J* 86(3):1829–1842.